ELSEVIER

International Journal of Heat and Fluid Flow 21 (2000) 271–277

International Journal of HEAT AND FLUID FLOW

www.elsevier.com/locate/ijhff

Turbulent structure in the three-dimensional boundary layer on a swept wing

Motoyuki Itoh [a,*], Minoru Kobayashi [b]

[a] *Department of Mechanical Engineering, Nagoya Institute of Technology, Gokiso-cho, Showa-ku, Nagoya, 466, Japan*
[b] *Nippon Sharyo, 1-1, Sanbonmatsu-cho, Atsuta-ku, Nagoya, Japan*

Received 30 August 1999; accepted 6 January 2000

Abstract

The effects of mean flow three-dimensionality on the turbulent structure of the boundary layer on a swept wing are investigated experimentally. The configuration of the test model used to simulate the infinite swept wing condition is similar to that used by Van den Berg, B., Elsenaar, A., Lindhout, J.P.F., Wesseling, P., 1975. Measurements in an incompressible three-dimensional turbulent boundary layer, under infinite swept-wing conditions, and comparison with theory. J. Fluid Mech. 70 (1), 127–148. Mean flow measurements show that the location of the maximum cross-flow velocity is within the log-law region for the streamwise velocity profiles. In the near-wall region, the streamwise turbulence intensity, $\sqrt{\overline{u^2}}/U_\tau$, decreases with increasing three-dimensionality. A four quadrant analysis is applied to the fluctuating velocity components in the local mean flow and wall-normal directions. At downstream stations, the contributions to the turbulent shear stress from quadrant 4 (sweeps) are predominant in the region near the wall. It is thus revealed that strong ejections are suppressed by the effects of increased three-dimensionality.

Keywords: Swept-back wing; Three-dimensional turbulent boundary layer; Turbulent structure; Near-wall region; Hot-wire anemometry; Four quadrant analysis

Notation

A_1	structure parameter
C_p	pressure coefficient, $2(P-P_0)/\rho U_0^2$
H	hole size for the quadrant analysis
P	static pressure
$\overline{q^2}/2$	turbulent kinetic energy, $(\overline{u^2}+\overline{v^2}+\overline{w^2})/2$
U_e	mean velocity of the free-stream
U_s, U_n	mean velocity components in the free-stream and cross-flow directions, respectively
U_τ	friction velocity
u, v, w	fluctuating velocity components in the streamwise, wall-normal and cross-flow directions, respectively
u^*	fluctuating velocity component in the local mean flow direction
x, y	parallel to the tunnel axis and wall-normal coordinates, respectively

Greeks

γ_i	intermittency factor of the ith quadrant
δ_{99}	boundary layer thickness
ν	kinematic viscosity of the working fluid
ρ	density of the working fluid
τ_w	wall shear stress
φ	flow angle measured relative to the local free-stream

Superscript

+	dimensionless quantity scaled with ν and U_τ

1. Introduction

Many engineering boundary layer flows, such as those over swept wings, within turbomachinery and over hulls of ships, are turbulent and three-dimensional. There have been many experimental and theoretical works on the three-dimensional turbulent boundary layers (see reviews by Bradshaw, 1987; Johnston and Flack, 1996). In those investigations, several basic differences were found between two- and three-dimensional turbulent boundary layers. One of them is that the direction of the shear-stress does not align with the direction of the velocity-gradient vector. Another important difference is that the structure parameter A_1 is smaller for three-dimensional boundary layers than for two-dimensional ones. However, the causal structural changes are not fully understood.

Eaton (1995) reviewed several experiments and simulations examining the near-wall structure of three-dimensional

* Corresponding author. Tel.: +81-52-735-5328; fax: +81-52-735-5342.
E-mail address: mitoh@megw.mech.nitech.ac.jp (M. Itoh).

0142-727X/00/$ - see front matter
PII: S0142-727X(00)00009-6

turbulent boundary layers and concluded that it is appropriate to interpret the structure of the three-dimensional turbulent boundary layer as a distorted version of the two-dimensional one, i.e., low- and high-speed streaks and quasi-streamwise vortices dominate the flow near the wall (Robinson, 1991). Chiang and Eaton (1996) and Flack (1997) studied the near-wall structures of three-dimensional turbulent boundary layers using flow visualization techniques. Their conclusions, however, were contradictory in that asymmetry of the near-wall structure, found by Chiang and Eaton (1996) was not observed in Flack's experiments (1997).

In the present work, a three-dimensional turbulent boundary layer was produced in a model similar to that used by van den Berg et al. (1975). Measurements of the mean velocity profiles and the Reynolds stresses were obtained by the use of hot-wire anemometry. The mean velocity distributions obtained are discussed in view of the theoretical predictions of Degani et al. (1993). To study the effects of mean flow three-dimensionality on the structure of turbulence, a four-quadrant analysis was applied to the u^*- and v-components, where u^* and v represent the fluctuating velocity components in the local mean flow and wall-normal directions, respectively.

2. Experimental apparatus and procedure

Experiments were performed in a low-speed wind tunnel at the Nagoya Institute of Technology. The model (Fig. 1) used to simulate the boundary layer on an infinite swept wing is similar to that used by van den Berg et al. (1975) at NAL in The Netherlands. The model was installed in the working section ($800 \times 800 \times 3000$ mm^3) of the wind tunnel. The leading edge of the flat test plate was swept at 35° with respect to the direction of the oncoming free stream. A 1.6 mm trip wire was glued on the test plate at 50 mm downstream of the leading edge. In order to obtain the required pressure distribution to the test plate (i.e., a constant pressure along the generator on the test plate) as accurately as possible, the ingenious contrivances used by van den Berg et al. (1975) were adopted here also. The only novel design in the present model was the flat roof and side walls extending upstream of the flexible roof, and the curved side walls. With these extended walls, the mean flow two-dimensionality was more closely approximated at the upstream measuring stations ($x = -108$ mm) than with the configuration without the walls. The infinite-swept condition was approximated by adjusting the pressure-inducing roof, the curved side walls and a blockage attached to the downstream end of the model (see Fig. 1). The upstream ends ($x = 0$) of the flexible roof and the curved side walls were situated at 400 mm downstream of the leading edge of the flat test plate.

Velocity measurements were carried out in the boundary layer on the flat test plate at 5 stations ($x = -108$, 108, 252, 396, 540 mm) along a line parallel to the tunnel axis. Two types of single-wire (hot-wire) probes were used (Itoh et al., 1989). One had a wire normal to the rotation axis and was used for the mean flow measurements as well as Reynolds stresses $\overline{u^2}$ and $\overline{w^2}$, where u and w represent the fluctuating velocity components in the local free-stream and cross-flow directions, respectively. The other had a wire inclined at an angle of about 45° to its rotation axis and was used for measurements of Reynolds stresses $\overline{v^2}$, $\overline{uv}$ and $\overline{vw}$. The hot-wire was 3.1 μm in diameter, made of tungsten and copper plated at both ends, with an active length $\ell = 0.5$ mm (see ℓ^+ in Table 1). To measure the two instantaneous velocity components in the local mean flow and wall-normal directions, an X-wire probe was used. The two wires of the X-wire probe were separated by 0.3 mm. Wall shear stress τ_w was evaluated from the mean velocity gradient in the viscous sublayer. To determine this gradient, the measurements of mean velocity distribution were made down to the wall-normal distance $y \sim 0.05$ mm. Since

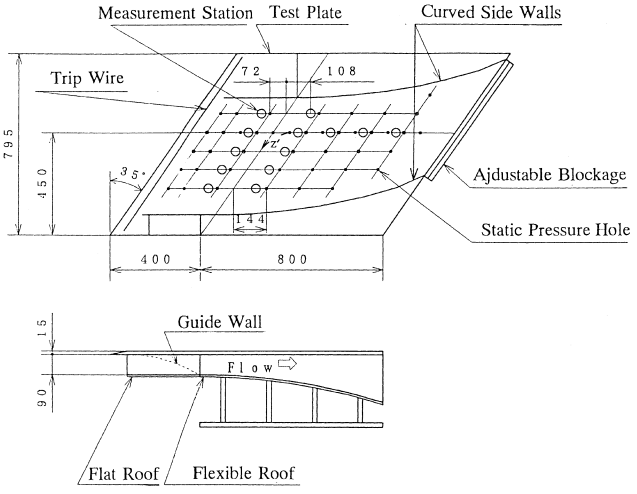

Fig. 1. Sketch of the model employed for boundary layer measurements.

Table 1
External-stream and boundary layer parameter[a]

x (nm)	U_e (m/s)	U_τ (m/s)	$\phi_w - \phi_e$	C_f	P^+	Re_θ
−108	15.4	0.739	0.5	4.60×10^{-3}	-1.97×10^{-3}	1240
108	14.3	0.622	3.2	3.62×10^{-3}	3.55×10^{-3}	1620
252	13.5	0.533	6.4	3.10×10^{-3}	7.11×10^{-3}	2330
396	12.6	0.432	14.2	2.36×10^{-3}	1.22×10^{-3}	3520
540	11.9	0.379	28.6	2.02×10^{-3}	1.16×10^{-3}	5830

x (nm)	δ_{99} (mm)	δ^*(mm)	θ (mm)	H_{12}	ℓ^+
−108	12.6	1.69	1.24	1.32	24.0
108	16.4	2.39	1.72	1.39	20.5
252	21.6	3.78	2.63	1.44	17.5
396	31.8	6.65	4.29	1.55	14.1
540	47.1	11.6	7.33	1.58	12.6

[a] $P^+ = \nu/\rho U_\tau^3 \partial P/\partial x$ $\ell^+ = U_\tau l/\nu$.

heat conduction to the wall caused erroneous hot-wire readings near the wall itself, a similar procedure to that used in our previous work (Itoh et al., 1992) was adopted to correct the near-wall data. The free stream velocity flowing into the model was kept constant (15 m/s) throughout the present study.

The uncertainty for the velocity data was estimated to be ± 0.01 for the nondimensional mean velocity components U_s/U_e and U_n/U_e, ± 0.05 for $\sqrt{\overline{u^2}}/U_\tau$ and $\sqrt{\overline{w^2}}/U_\tau$, and ± 0.07 for $\overline{v^2}/U_\tau^2$ and $\overline{u^+v}/U_\tau$. The uncertainty in τ_w was estimated at $\pm 8\%$ of its absolute value.

3. Results and discussion

3.1. Surface pressure distributions

The local coefficient of pressure C_p was defined as

$$C_p = 2(P - P_0)/\rho U_0^2, \tag{1}$$

where P is the local wall static pressure, P_0 is P at the reference station ($x = 0$) and U_0 is the velocity of the oncoming uniform free stream.

The static pressure distributions along the generators are shown in Fig. 2. The approximation to the infinite swept wing condition is comparable to that of van den Berg et al. (1975). Fig. 3 shows the static pressure distribution parallel to the tunnel axis. For comparison, the corresponding pressure distributions in the experiments of van den Berg et al. (NLR) and Bradshaw and Pontikos (1985) are shown in the same figure.

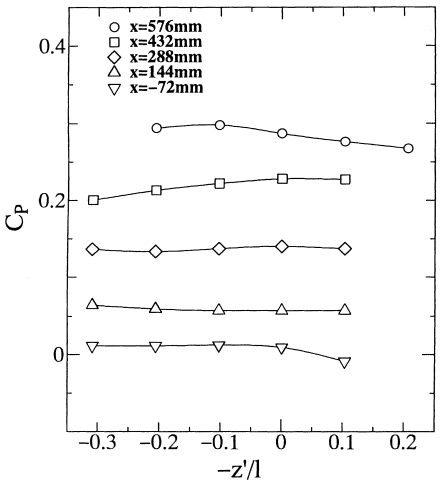

Fig. 2. Surface-pressure distributions parallel to leading edge of test plate.

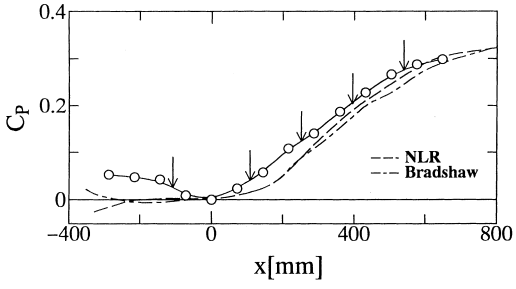

Fig. 3. Surface-pressure distributions parallel to tunnel axis.

The velocity measurement stations are indicated by arrows. Note that a favorable pressure gradient is obtained at the most upstream velocity measurement station ($x = -108$ mm), and that values of the nondimensional (adverse) pressure gradient P^+ at two downstream stations ($x = 396$ and $x = 540$ mm) are nearly equal to each other (see Table 1). The latter situation seems to be useful, at least for the near-wall region, in discerning the effects of three-dimensionality from those of the adverse pressure gradient.

3.2. Mean flow field

Fig. 4 shows the mean velocity distributions, where U_s and U_n are the mean velocity components in the free-stream and cross-flow directions, respectively. Both velocity components are normalized by the free-stream velocity at the outer edge of the boundary layer U_e. It should be noted that the peaks of the U_n-profiles are very close to the wall. Due to the adverse pressure gradient, as seen in Fig. 3, the shape of the U_s profile becomes more and more decelerated in the downstream direction. Flow angles measured relative to the local free-stream direction, $\varphi - \varphi_e$, are shown in Fig. 5. The maximum skew

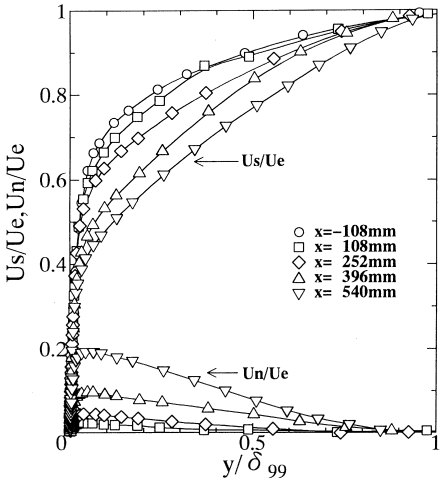

Fig. 4. Mean velocity distributions.

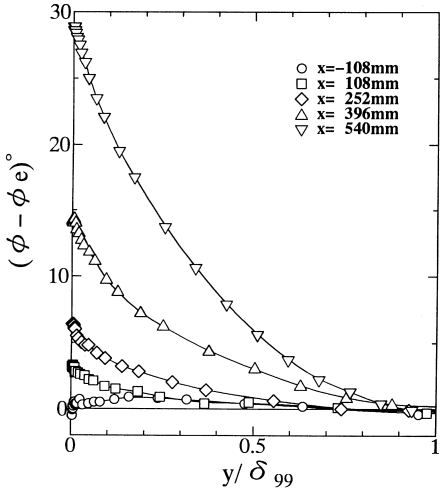

Fig. 5. Directions of velocity in boundary layer.

angle is around 30°, which is between those of van den Berg et al. (1975) and Bradshaw and Pontikos (1985). The turning angle of the free-stream, φ_e, was less than 10° (in reference to the tunnel axis) at the most downstream velocity measurement station ($x = 540$ mm). Values of the traditional integral parameters are shown in Table 1, together with other boundary layer parameters, where C_f is the skin friction coefficient ($C_f = 2\tau_w/\rho U_e^2$). The boundary layer thickness δ_{99}, the displacement thickness δ^* and the momentum thickness θ are defined based on the U_s-profiles. The shape factor H_{12} and the Reynolds number Re_θ are defined as $H_{12} = \delta^*/\theta$ and $Re_\theta = U_e\theta/\nu$, respectively.

Fig. 6 shows the polar plots of the mean velocity distributions. The straight lines radiating from the origin represent the directions of wall shear stress at respective stations. The collateral flow in the near-wall region, where the data are on straight lines, was found to extend only up to $y^+ = 5 \sim 10$.

The log-law plots for the mean velocity components U_s and U_n are shown in Fig. 7, where $(\varphi_w - \varphi_e)$ represents the angle between the directions of the wall shear stress and the local free-stream. It is evident in the figure that, going downstream, the area of the collateral flow in the near-wall region increases

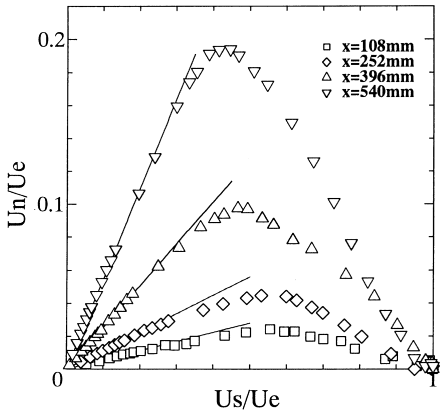

Fig. 6. Polar plots of velocity distributions.

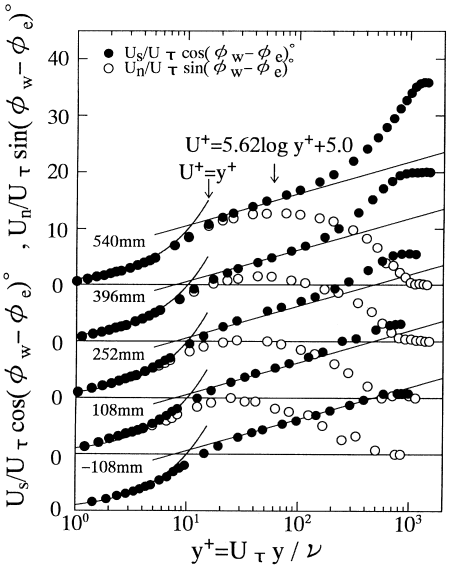

Fig. 7. Log-law plot of mean velocity components.

and the location of the maximum U_n shifts outward from the wall. A log-law region is apparent for the U_s-component but not for the U_n-component, probably because the Reynolds number is not large enough. The location of the maximum U_n is within the log-law region for the U_s-component. All these results are in accordance with the theoretical predictions of Degani et al. (1993). Furthermore, one should note that the log-law region for the U_s-profiles can be described by the expression established for the flat plate boundary layer.

3.3. Turbulence field

Fig. 8 shows the turbulence intensities $\sqrt{\overline{u^2}}$ and $\sqrt{\overline{w^2}}$. In the outer region ($y^+ > 200$), both $\sqrt{\overline{u^2}}/U_\tau$ and $\sqrt{\overline{w^2}}/U_\tau$ increase in the downstream direction. This may be ascribable to the effect of the adverse pressure gradient (Nagano et al., 1992). It should be remarked that, in the near-wall region, $\sqrt{\overline{u^2}}/U_\tau$ decreases appreciably while going downstream from $x = 396$ to $x = 540$ mm. This seems to be due to the effects of increased three-dimensionality. On the other hand, $\sqrt{\overline{w^2}}/U_\tau$ increases even in the near-wall region while going downstream from $x = 396$ to $x = 540$ mm, as seen in Fig. 8(b). These results are consistent with numerical predictions (Moin et al., 1992) of the effects of three-dimensionality on the turbulence statistics.

The wall-normal turbulence intensity $\sqrt{\overline{v^2}}$ is shown in Fig. 9. As we used an X-wire probe to obtain $\sqrt{\overline{v^2}}$-values, the data in the near-wall region could not be obtained. The increase in $\sqrt{\overline{v^2}}/U_\tau$ in the downstream direction seems to be due to the dominant effect of the adverse pressure gradient (Nagano et al., 1992).

Fig. 10 shows the turbulent shear stress $-\overline{u^*v}$, where u^* is the turbulent velocity component in the local mean flow direction. It should be noted that, in the region $y/\delta_{99} < 0.4$, the value of $-\overline{u^*v}/U_\tau^2$ decreases downstream from $x = 396$ to $x = 540$ mm. This seems to be due to the effects of increased three-dimensionality.

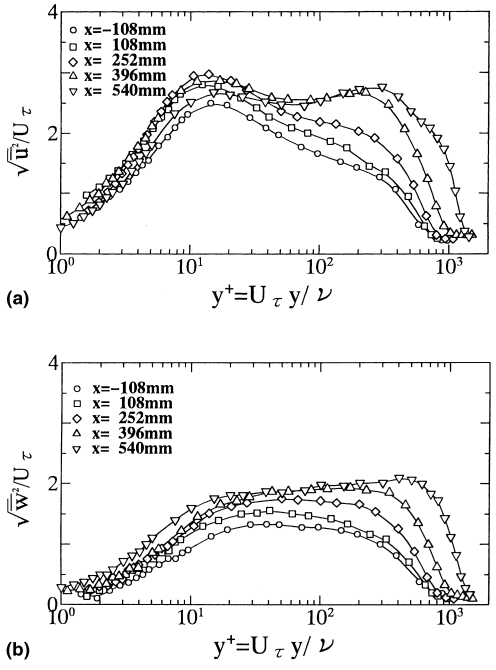

Fig. 8. Distributions of turbulence intensities: (a) streamwise component (b) cross-flow component.

Although all the components of Reynolds shear stress were obtained using a rotated hot-wire, they will not be discussed here any further because the main concern in the present study is to clarify the causes for the decreasing structure parameter, A_1, with increasing three-dimensionality.

The distributions of the turbulent kinetic energy, $\overline{q^2}/2$, are shown in Fig. 11. The values of $\overline{q^2}/U_\tau$ near the wall decrease downstream from $x = 396$ to $x = 540$ mm, which also seems to be due to the effects of increased three-dimensionality.

Fig. 12 shows the distributions of the structure parameter A_1 (ratio of shear-stress magnitude in the plane parallel to the wall to twice the turbulent kinetic energy). As is well known, the value of A_1 decreases with increasing three-dimensionality. In Fig. 12, A_1 decreases from about 0.15 (at $x = -108$) to 0.11 (at $x = 540$ mm) in the central region of the boundary layer.

Fig. 13(a) and (b) show the turbulent transport of the turbulence energy component u^{*2} and the turbulent shear stress $\overline{u^*v}$. It is seen in Fig. 13(a) that in the downstream direction the values of $\overline{vu^{*2}}/U_\tau$ decrease near the wall and become negative at the stations $x = 396$ and $x = 540$ mm. The negative values of

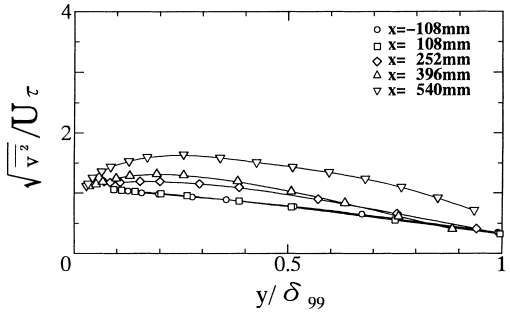

Fig. 9. Wall-normal component of turbulence intensity.

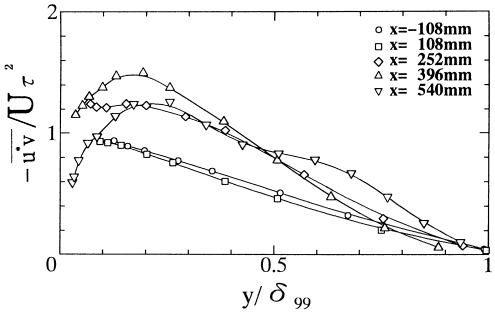

Fig. 10. Turbulent shear stress.

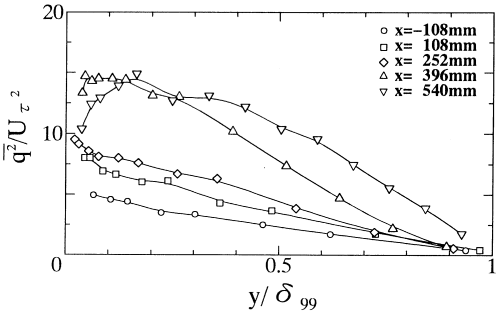

Fig. 11. Distributions of turbulent kinetic energy.

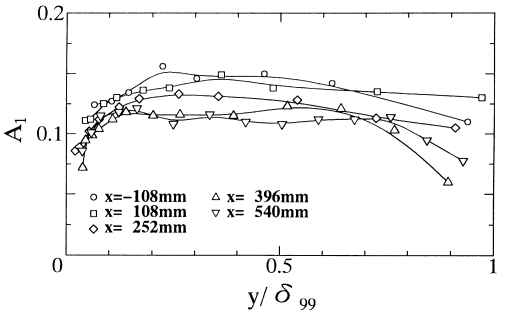

Fig. 12. Distributions of structure parameter A_1.

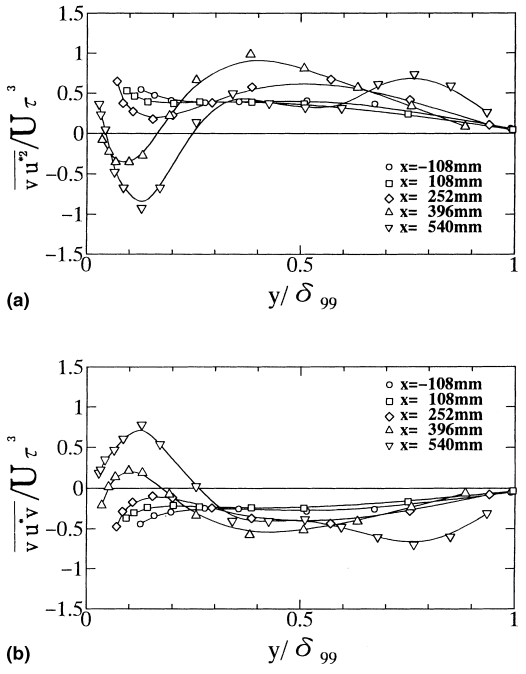

Fig. 13. Distributions of turbulent transport: (a) $\overline{u^{*2}}$; (b) $\overline{u^*v}$.

$\overline{vu^{*2}}/U_\tau$ indicate that the turbulence energy $\overline{u^{*2}}$ is transported toward the wall. It can be seen from Fig. 13(b) that the turbulent transport of $-\overline{vu^{*2}}$ is also toward the wall in the same region as for $\overline{u^{*2}}$. A wallward turbulent transport has also been found in turbulent boundary layers with adverse pressure gradients (Nagano et al., 1992; Krogstad and Skare, 1995).

3.4. Four quadrant analysis

To investigate the effects of mean flow three-dimensionality on turbulence producing events near the wall, a four quadrant analysis (Lu and Willmarth, 1973) was applied to the u^* and v components. The fractional contributions to the Reynolds stress $-\overline{u^*v}$ from respective quadrants (i) in the u^*–v plane are shown in Fig. 14 for $x = 540$ mm. The parameter H is a threshold defined by $H = |u^*v|/\sqrt{\overline{u^{*2}}}\sqrt{\overline{v^2}}$, commonly called "hole size". For evaluating strong events, the data with $H = 2$ are also shown as well as those with $H = 0$. It was observed that, at the upstream stations ($x \leqslant 252$ mm), the contribution from quadrant 2 ($Q2$) is the largest of all across the boundary layer. However, at the downstream stations ($x \geqslant 396$ mm), the fractional contribution from $Q2$ is reduced markedly near the

wall, with the contribution from $Q4$ instead predominating, as seen in Fig. 14. Similar results were reported for boundary layers with a strong adverse pressure gradient (Krogstad and Skare, 1995). The ratio of contributions to $-\overline{u^*v}$ from $Q2$ and $Q4$ are shown in Fig. 15. It is noted that the $Q4$ events (sweeps) are predominant in the region where wallward turbulent transport is observed in Fig. 13. It should be remarked that a plateau region exists in the central part ($0.35 < y/\delta_{99} < 0.55$) of the curve for the most downstream station ($x = 540$ mm).

Fig. 16 shows the intermittency factor γ_i for $x = 540$ mm. It was found, by comparing these data with those for the upstream stations (not shown here), that γ_i-values for $i = 2$ with $H = 2$ (or $i = 4$ with $H = 0$) decrease going downstream near the wall. The ratio of γ_i for $Q2$ and $Q4$ events with $H = 2$ are shown in Fig. 17. Note that a qualitative agreement is obtained between Figs. 15 and 17.

Fig. 18 shows the mean time intervals between ejections ($\overline{T^+}_2$) or sweeps ($\overline{T^+}_4$) with $H = 2$, where $\overline{T^+} = \overline{T}U_\tau^2/\nu$. $\overline{T^+}_2$ noticeably decreases in the downstream direction at the upstream stations, but increases from $x = 396$ to $x = 540$ mm. This remarkable finding suggests that strong ejections are suppressed by the effects of increased mean flow three-dimensionality. As we have not visualized the near-wall structure, it is not known whether one vortex sign produces ejections that are considerably weaker than the other sign (namely, asymmetry of the near-wall structure (Chiang and Eaton, 1996) in the region of increased three-dimensionality.

The mean durations of $Q2$ and $Q4$ events with $H = 2$ are shown in Fig. 19. As seen in the figure, the normalized mean durations of both events (strong ejections and sweeps) decrease going downstream, and the difference between the durations of ejections and sweeps becomes smaller.

Fig. 20 shows the conditional averages of u^*,v and $-u^*v$ normalized with their rms values. Although the u^*-pattern changes little, the width at half-height of the v-and u^*v-patterns is reduced as the mean flow three-dimensionality increases. It is noted that the $(-uv)'$-values at far from the detection time ($T^+ = 0$) are rather small at $x = 540$ mm. These results may

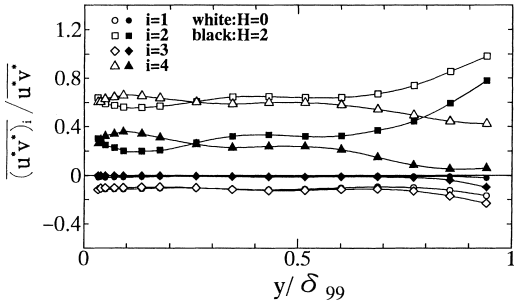

Fig. 14. Fractional contributions to $-\overline{u^*v}$ from respective quadrants in u^*-v plane at $x = 540$ mm.

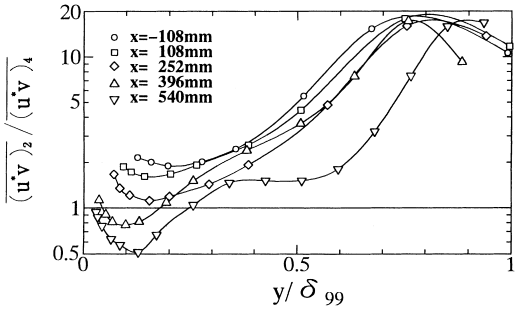

Fig. 15. Ratio of the contributions to $-\overline{u^*v}$ from $Q2$ to $Q4$ with $H = 2$.

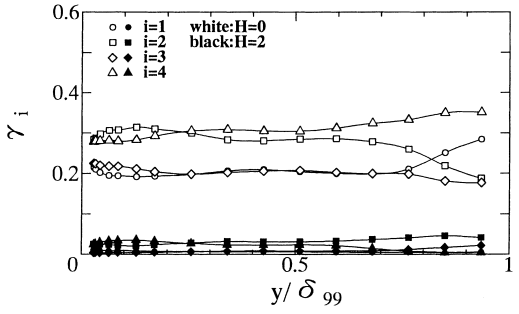

Fig. 16. Intermittency factor of respective events at $x = 540$ mm.

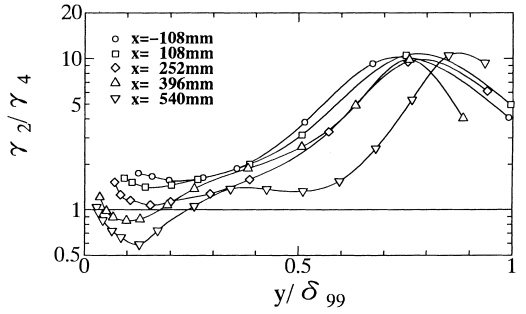

Fig. 17. Ratio of the intermittency factors of $Q2$ and $Q4$ with $H = 2$.

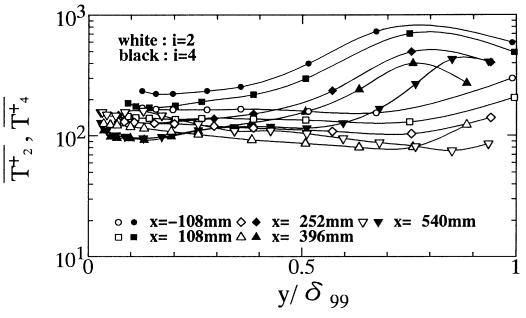

Fig. 18. Time intervals of $Q2$ and $Q4$ events with $H = 2$.

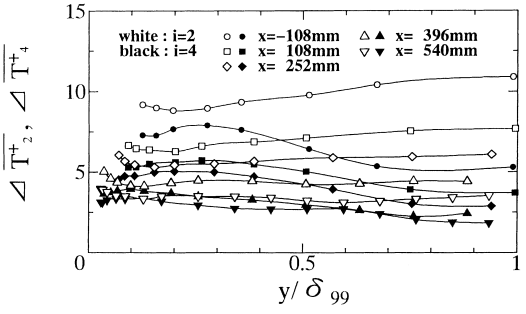

Fig. 19. Mean duration of respective events with $H = 2$.

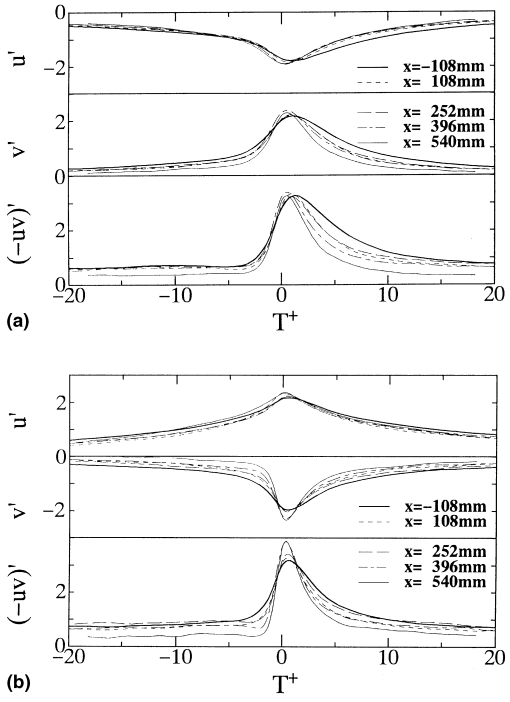

Fig. 20. Conditional averages of u^*, v and $-u^*v$ with $H = 2$ at $y^+ \sim 50$: (a) ejections; (b) sweeps.

explain some aspects of the reduction in $\overline{(-uv)'}$ with increasing three-dimensionality.

4. Conclusions

An experimental study was made of the turbulent structure of the three-dimensional boundary layer on an infinite swept wing. The results obtained are summarized as follows.

1. The location of the maximum U_n is within the log-law region of U_s-profiles, where U_n and U_s represent the mean velocity components in the cross-flow and local free-stream directions, respectively.
2. In the near-wall region, the streamwise turbulence intensity, $\sqrt{\overline{u^2}}/U_\tau$, decreases with increasing mean flow three-dimensionality. In contrast, the cross-flow component, $\sqrt{\overline{w^2}}/U_\tau$, increases.
3. At downstream stations, the turbulent transport to the wall was observed in the near-wall region where sweeps were dominant.
4. A four quadrant analysis suggests that strong ejections are suppressed by the effects of increased three-dimensionality.

References

Bradshaw, P., Pontikos, N.S., 1985. Measurements in the turbulent boundary layer on an infinite swept wing. J. Fluid Mech. 159, 105–130.

Bradshaw, P., 1987. Turbulent secondary flows. Ann. Rev. Fluid Mech. 19, 53–74.

Chiang, C., Eaton, J.K, 1996. An experimental study of the effects of three-dimensionality on the near wall structures using flow visualization. Exp. Fluids 20, 266–272.

Degani, A.T., Smith, F.T., Walker, J.D.A., 1993. The structure of a three-dimensional turbulent boundary layer. J. Fluid Mech. 250, 43–68.

Eaton, J.K., 1995. Effects of mean flow three-dimensionality on turbulent boundary-layer structure. AIAA J. 33 (11), 2020–2025.

Flack, K.A., 1997. Near-wall structure of three-dimensional turbulent boundary layers. Exp. Fluids 23, 335–340.

Itoh, M., Yamada, Y., Suzuki, H., 1989. Experiments on the turbulent boundary layers on spinning cones in axial flow. In: Proceedings of the Seventh Symposium on Turbulent Hear Lows, vol. 2, pp. 2.1.1.1–2.1.1.6.

Itoh, M., Yamada, Y., Imao, S., Gonda, M., 1992. Experiments on turbulent flow due to an enclosed rotating disk. Exp. Therm. Fluid Sci. 5 (3), 359–368.

Johnston, J.P., Flack, K.A., 1996. Review-advances in three-dimensional turbulent boundary layers with emphasis on the wall-layer regions. J. Fluid Eng. 118, 219–232.

Krogstad, P.-A., Skare, P.E., 1995. Influence of a strong adverse pressure gradient on the turbulent structure in a boundary layer. Phys. Fluids A 7 (8), 2014–2024.

Lu, S.S., Willmarth, W.W., 1973. Measurements of the structure of the Reynolds stress in a turbulent boundary layer. J. Fluid Mech. 60 (3), 481–511.

Moin, P., Shih, T.H., Driver, D., Mansour, N.N., 1992. Direct numerical simulation of a three-dimensional turbulent boundary layer. Phys. Fluids A 2 (10), 1846–1853.

Nagano, Y., Tagawa, M., Tsuji, T., 1992. Effects of adverse pressure gradients on mean flows and turbulence statistics in a boundary layer. Turbulent Shear Flows 8, 7–22.

Robinson, S.K., 1991. Coherent motions in the turbulent boundary layer. Ann. Rev. Fluid Mech. 23, 601–639.

Van den Berg, B., Elsenaar, A., Lindhout, J.P.F., Wesseling, P., 1975. Measurements in an incompressible three-dimensional turbulent boundary layer, under infinite swept-wing conditions, and comparison with theory. J. Fluid Mech. 70 (1), 127–148.